Journal of Membrane Science 327 (2009) 87–95

Contents lists available at ScienceDirect

Journal of Membrane Science

journal homepage: www.elsevier.com/locate/memsci

Combined fouling of nanofiltration membranes: Mechanisms and effect of organic matter

Alison E. Contreras [a], Albert Kim [b], Qilin Li [a,*]

[a] Department of Civil and Environmental Engineering, Rice University, Houston, TX, 77005, United States
[b] Department of Civil and Environmental Engineering, University of Hawaii at Manoa, Honolulu, HI 96822, United States

ARTICLE INFO

Article history:
Received 3 September 2008
Received in revised form 7 November 2008
Accepted 8 November 2008
Available online 27 November 2008

Keywords:
Nanofiltration
Combined fouling
Foulant interactions
Colloids
Organic foulant

ABSTRACT

The accurate prediction of nanofiltration membrane performance in industrial applications is dependent upon understanding the fouling behavior of representative feed solutions. However, most membrane studies focus on fouling of a single type of foulant, which is not a good predictor for realistic feed solutions that contain multiple foulant types. In this study, combined fouling by organic and inorganic colloidal foulants is studied. Through the use of model foulants, three hypothesized mechanisms responsible for the enhanced membrane flux decline in the presence of multiple foulant types are examined: increased hydraulic resistance of the mixed cake layer structure, hindered foulant diffusion due to interactions between solute concentration polarization layers, and changes in colloid surface properties due to organic adsorption. All three mechanisms were found to play a role in combined fouling to various degrees. Organic adsorption was shown to cause the greatest synergistic effect. The synergistic effect caused by increased resistance of a heterogeneous fouling layer indicates that current fouling layer models need to be reexamined to include the suggested mechanisms.

1. Introduction

Nanofiltration (NF) is an attractive technology for producing clean water from non-traditional sources, i.e. brackish water and wastewater, since it can provide high multivalent ion and organic contaminant rejection at a much lower operating pressure than reverse osmosis. Unfortunately, as with all membrane filtration processes, an inherent problem of NF is decreased productivity due to fouling of the membrane by colloidal materials, dissolved organics, inorganic precipitates, and microorganisms. While fouling can be controlled by using low fouling membrane materials [1–4], pre-treatment of the feed stream [5–8], and optimizing the system configuration and operation [9,10], proper use of these control strategies still requires a deeper understanding of the responsible fouling mechanisms.

Most previous studies on membrane fouling have focused only on a single, well characterized foulant of homogenous physicochemical properties (referred to in this paper as individual fouling). One marked limitation in applying the theoretical and experimental results obtained from these studies to water and wastewater filtration systems is that fouling in these systems is almost always caused by more than one type of foulant with various particle sizes and surface characteristics, most commonly both colloidal materials and dissolved organic macromolecules, e.g., natural organic matter (NOM) and soluble microbial products. Several studies have identified that poly-dispersed suspensions form cake layer structures with resistances different than mono-dispersed solutions and that interactions between foulants can be correlated to flux decline behavior [11–14].

A limited number of studies on combined fouling (i.e., fouling with multiple types of foulants) by both inorganic colloids and dissolved organic matter have shown that fouling behavior differs under varying solution conditions and with different membrane types [15–17]. Li and Elimelech [16] performed combined fouling experiments with a low salt rejection NF membrane in the presence of silica colloids and NOM. Flux measurements revealed significantly faster membrane fouling in combined fouling experiments than what might be predicted by summing the contributions from each foulant based on the individual fouling experiments. The aggravated membrane fouling or enhanced flux decline, referred to as a synergistic effect, was attributed to the hindered back diffusion of each foulant. In another study performed on a high salt rejection NF membrane, Lee et al. [15] found that flux decline during filtration of a mixture of NOM and silica colloids was initially greater than the sum of the flux declines caused by each foulant individually, but was reduced in the latter filtration stages. It was hypothesized that an "active salt rejecting layer" formed during combined fouling negated the effect of cake-enhanced concentration polarization (CECP), which increases the salt concentration and

* Corresponding author. Tel.: +1 713 348 2046; fax: +1 713 348 2026.
E-mail addresses: Alison.Contreras@rice.edu (A.E. Contreras), Albert.S.Kim@hawaii.edu (A. Kim), qilin.li@rice.edu (Q. Li).

0376-7388/$ – see front matter © 2008 Elsevier B.V. All rights reserved.
doi:10.1016/j.memsci.2008.11.030

consequently the osmotic pressure in the concentration polarization (CP) layer of salt ions [9,18]. It is important to note that although fouling behavior differed according to the experimental conditions of each study, common throughout these studies is the observation that combined fouling cannot be predicted from fouling by individual foulants alone.

The objective of this study was to understand the effects of different organic foulants found in water and wastewater on combined fouling during the nanofiltration of complex solutions containing both colloidal materials and dissolved organic matter. Interactions of four model organic macromolecules with colloidal silica foulants and the membrane surface were thoroughly characterized and related to membrane flux behavior observed in cross-flow filtration experiments to reveal the different combined fouling mechanisms involved. Results of the study clearly demonstrated the significance of interactions among different foulant types, which has been largely neglected in previous mechanistic studies.

2. Theory

Three potential mechanisms have been identified as contributing to the combined fouling flux decline observed during previous combined fouling studies [15–17]. The weighted effect of each mechanism is anticipated to be different for interacting vs. non-interacting foulants.

2.1. Increased cake layer resistance

Dissolved organic compounds in water and wastewater are much smaller in size compared to colloidal foulants such as silica. It has been shown that poly-dispersity in particle size distribution is likely to affect fouling layer resistance by altering the structure of the cake/gel layer formed at the surface of the membrane [11,19,20].

Membrane permeate flux can be described by the resistance in series model:

$$v = \frac{\Delta P - \Delta\pi_m}{\mu(R_m + R_c)} \tag{1}$$

where v is the permeate flux, ΔP is the applied pressure, $\Delta\pi_m$ is the trans-membrane osmotic pressure, μ is the dynamic viscosity of the solution, R_m is the resistance of the membrane and R_c is the resistance of the cake/gel layer. R_c is determined by the specific resistance of the fouling layer or the fouling layer mass per membrane unit area. For mono-dispersed, spherical colloids, the specific cake resistance is usually estimated using the Carman–Kozeny equation,

$$\hat{R}_c = \frac{180\mu(1-\varepsilon_c)}{\rho_p d_p^2 \varepsilon_c^3} \tag{2}$$

where ε_c is cake layer porosity, ρ_p is solid density of the particle, and d_p is particle diameter. The Carman–Kozeny equation predicts that decreases in cake porosity and particle diameter result in an increase in the specific cake layer resistance. Although this equation is only applicable for rigid, nearly touching particles, one can imagine that as the porosity of the layer decreases due to the presence of smaller particles filling interstitial pore spaces, as shown in Fig. 1, the same relation would be true for the mixed fouling layer adjacent to the membrane. Fouling layer resistance would consequently increase, resulting in increased flux decline. A recent analytical study verified this theory by showing that a cake layer composed of normally distributed particle sizes will always create a higher specific resistance compared to a log-normal distribution with the same mean particle size due to the presence of more small particles in the normal distribution [19].

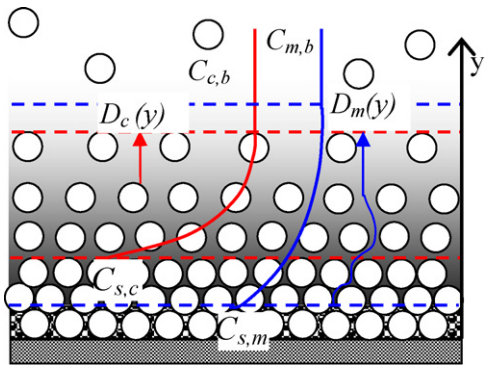

Fig. 1. Schematic description of the cake/gel and CP layers of colloids and macromolecules after cake/gel layer formation. C_s: concentration at the membrane surface; C_b: bulk concentration; D: back diffusion coefficient. Subscript: c = colloids, m = macromolecules.

2.2. Hindered back diffusion

The back diffusion of one foulant type may be hindered by the presence of the concentration polarization of fouling layer of other types of foulants. During filtration, permeate flow brings the solute towards the membrane surface, convective flow transports the solute along the membrane surface tangentially, and Brownian diffusion and shear-induced diffusion simultaneously transport the solute back to the bulk fluid. Recently, the Brownian and shear-induced diffusion phenomena were unified using irreversible thermodynamics [21]. For small particles ($\ll$1 μm), such as the colloidal particles used in this study, shear-induced diffusion is negligible [22]. Accumulation of the solute within the concentration polarization layer can be described by the convective-diffusion equation,

$$\frac{\partial C}{\partial t} + \vec{v}_w \cdot \nabla C - \nabla(D\nabla C) = 0 \tag{3}$$

where D is the back diffusion coefficient, v_w is the flow velocity, and C is the concentration of the solute. A schematic description is available in Fig. 1.

The Stokes–Einstein equation (Eq. (4)) can be used to estimate the diffusion coefficient of small, spherical solutes in free solution

$$D_o = \frac{k_B T}{3\pi\mu d_p} \tag{4}$$

where k_B is the Boltzmann constant and T is the absolute temperature. When there is significant accumulation of colloids at the membrane surface, i.e. formation of a cake layer, back diffusion of smaller solutes, e.g., dissolved organic foulants, is hindered by the presence of the cake layer due to the tortuous pathway of transport. The hindered diffusion coefficient D^* is related to the porosity (ε) and diffusive tortuosity (τ) of the cake layer [18].

$$D^* = \frac{D_o \varepsilon}{\tau^2} \tag{5}$$

The slower back diffusion leads to faster accumulation of the smaller solutes and hence a higher concentration in the CP layer. This phenomenon has been demonstrated with salt ions – termed cake-enhanced concentration polarization (CECP) – and has been identified as a significant contributor to membrane flux decline observed in colloidal fouling of NF and RO membranes [9,18]. CECP is observed by a decrease in the observed salt rejection over time as the concentration of salt at the membrane surface increases.

CECP may also occur for dissolved organic compounds that are small enough to penetrate the colloidal cake layer. As a result, the concentration of dissolved organic foulants in the CP layer is increased and formation of the organic gel layer is accelerated.

Meanwhile, the higher organic concentration in the CP layer increases local fluid viscosity. Although only valid at dilute concentrations, the Stokes–Einstein equation predicts that the diffusivity of colloids will be reduced as the local fluid viscosity increases, further accelerating colloidal foulant accumulation at the membrane surface. In reality, higher concentrations at the membrane surface will make colloid–colloid interactions and volume exclusion more important.

2.3. Alteration of colloid surface properties due to adsorption of dissolved organic macromolecules

Adsorption of dissolved macromolecules on colloidal surfaces can disturb electric double layer interactions and alter van der Waals forces among colloids and between colloids and membranes, as well as cause steric hindrance effects. A number of studies on colloidal transport in porous media have shown that NOM can play an important role in facilitating the transport of natural and model colloids [23–25] and their aggregation kinetics [26]. Additionally, interactions between the organic foulant and the membrane surface can modify membrane surface properties, including membrane surface roughness, hydrophobicity and charge, and has been shown to affect flux behavior [27–30]. These changes can significantly modify the fouling behavior of colloidal particles by either increasing or decreasing (depending on the molecular characteristics of the organic foulant) colloidal aggregation in the CP layer and their deposition on the membrane surface.

3. Materials and methods

3.1. NF membrane

A low salt-rejection thin-film composite nanofiltration membrane (NF 270 by Dow-FilmTec, Minneapolis, MN) was used in all filtration experiments. Precut membrane samples were stored in de-ionized water at 4 °C. The storage water was replaced weekly. The hydraulic resistance of the NF 270 membrane, determined from clean water flux measurements, was 1.98 ($\pm$0.09) $\times$ 10^{13} m^{-1} at 20 $\pm$ 0.3 °C. Observed salt rejection with 10 mM NaCl ranged from 40.2 to 58.8% at 20 $\pm$ 0.3 °C, consistent with the manufacturer's specified salt rejection of 40–60%. Membrane surface zeta potential was characterized using a streaming potential analyzer (Zeta CAD, CAD Instrumentation, Les Essarts le Roi, France). Measurements were performed under the various solution conditions used in the filtration experiments. Before each measurement, the membrane coupons were soaked in 10 mM NaCl (the background electrolyte solution used in filtration experiments) for 24 h at 4 °C. Membranes were then allowed to equilibrate with the test solution for 30 min before the measurement was started.

3.2. Model foulants

Commercial colloidal silica, Snowtex-XL (ST-XL, Nissan Chemical America Corp., Houston, TX) was used as the model colloidal foulant. Manufacturer supplied data specified that particle size ranged from 40 to 60 nm.

Humic substances, proteins and polysaccharides have been identified as the major organic foulants in water and wastewater [31–36]. For this reason, four organic compounds were used in this study: Suwannee River humic acid (HA), dextran, sodium alginate, and bovine serum albumin (BSA). In addition to the other commonly studied organic foulants, dextran was chosen because it is known to have minimum interaction with most surfaces and can serve as a good model for "non-interacting" macromolecules.

HA (standard II) was obtained from International Humic Substances Society (St. Paul, MN) and was not purified any further. Dextran from *Leuconostoc mesenteroides*, sodium alginate derived from brown algae, and BSA were purchased from Sigma–Aldrich (St. Louis, MO). The molecular weights reported by the manufacturers are 1–5, 9–11, 10–60, and ~66 kDa for humic acid, dextran, sodium alginate, and BSA, respectively. All stock solutions and feed waters were prepared using ultrapure water produced by a Millipore system (RiOS System, Billerica, MA). Because HA has low solubility under acidic conditions, pH was raised to 8.2 with NaOH and the solution was filtered using a vacuum filter (Whatman Grade No. 1 filter paper, England) and stored in an amber glass bottle. The concentration of the stock solution was then verified by total organic carbon (TOC) measurements with a TOC analyzer (Shimadzu Scientific Instruments, Japan). All stock solutions were stored in the dark at 4 °C.

Surface zeta potential and hydrodynamic diameter of the model foulants were characterized by electrophoretic mobility and dynamic light scattering (DLS) measurements using a Zetasizer Nano ZS (Malvern Instruments, Westborough, MA).

3.3. Measurement of organic foulant adsorption on silica

Adsorption of organic foulants on the silica colloidal particle surface determines their impact on colloid–colloid and colloid–membrane interactions. Adsorption of the model organic foulants on a silica surface was investigated using a quartz crystal microbalance with dissipation monitoring (QCM-D) technique (Q-Sense E4, Q-Sense, Glen Burnie, MD). Principles and applications of the QCM-D technique can be found elsewhere [37].

Silica-coated quartz crystals (QSX303, Q-Sense, Glen Burnie, MD) were used to simulate the surface of the model silica colloidal foulant. QCM-D measurements employed the same background solution (10 mM NaCl) and organic concentration (20 mg/L) used in the cross-flow filtration experiments. Before each experiment, the crystal sensors and the flow modules were cleaned with 2% sodium dodecyl sulfate (SDS) solution followed by de-ionized water and dried with ultrapure N_2 gas. The crystals were further cleaned in a UV/Ozone ProCleaner (BioForce Nanosciences, Ames, IA) for 20 min. In each experiment, fundamental frequencies of each crystal were first verified under dry air conditions. Then, a baseline was established by running the background solution (10 mM NaCl) for 10 min. This was followed by the adsorption phase using the organic foulant solution. After adsorption equilibrium was established, the influent was switched to the buffer solution again to remove the residual foulant solution in the cell channel.

3.4. Membrane filtration experiments

Nanofiltration experiments were carried out in a laboratory scale cross-flow membrane filtration system consisting of two membrane-cells in parallel [38]. A pulsation dampener (Model H1020V, Blacoh Fluid Control, Inc., Riverside, CA) situated at the outlet of the hydra-cell pump was charged at 80% operating pressure to dampen pressure irregularities. Feed water temperature was kept constant at 20 °C using a re-circulating water chiller (VWR, West Chester, PA).

Filtration experiments included three main phases: membrane compaction, conditioning, and fouling. The membranes were first compacted at 100 psi (689.5 kPa), a pressure higher than the designed experimental pressure, using ultrapure water for a minimum of 5 h to obtain a stable clean water flux. During the conditioning phase, background electrolyte solution, i.e. 10 mM NaCl was filtered through the membranes for at least 9 h. Pressure was adjusted to yield a stable permeate flux of 2×10^{-5} m/s in all experiments, corresponding to an applied pressure range of

65–70 psi (448–483 kPa). This ensured the same initial permeate flux for the fouling stage of all experiments. Conductivity of both permeate and feed waters was monitored during the conditioning phase to check membrane integrity and establish initial observed salt rejection. After a stable permeate flux of 2×10^{-5} m/s and appropriate salt rejection had been achieved, the fouling phase was started by addition of the corresponding foulant or foulants. The pump was stopped while the foulant was introduced to the feed tank and allowed to mix thoroughly for 5 min before pumping was resumed. A sample was taken from the feed reservoir immediately before filtration was resumed for confirmation of foulant concentration. Concentrations of colloidal and organic foulants used were 100 and 20 mg/L, respectively, in both individual fouling and combined fouling experiments. Pressure, permeate flux, and feed water temperature were continuously monitored during the experiments. Samples were taken from both the feed and permeate at predetermined times during both the conditioning and fouling stages for analysis of pH, conductivity (Oakton pH/CON 510 Benchtop Meter, Oakton Instruments, Vernon Hills, IL) and foulant concentrations. Concentrations of organic foulants were determined by TOC measurement. Colloidal foulant concentrations in the feed were determined by turbidity measurement using a turbidity meter (Hach Company, Loveless, CO). The cross-flow system was thoroughly cleaned after each experiment with 6 L of 5 mM NaOH re-circulated for 1 h followed by three rinses with 6 L of de-ionized water for at least 1 h each. All experiments were repeated at least twice.

4. Results and discussion

4.1. Characteristics of model foulants

The model foulants were characterized for their size and surface zeta potential under the solution conditions used in the filtration experiments. Table 1 summarizes the results of the characterization. The mean hydrodynamic diameter was derived from an average number-based-distribution based on at least five measurements. BSA has a negative surface zeta potential of -20.7 ± 0.9 mV under the experimental conditions used whereas that of dextran was close to neutral at -7.2 ± 1.5 mV. Alginate and HA had a much more negative zeta potential, measuring -45.0 ± 1.2 and -37.9 ± 1.2 mV, respectively, under the same solution conditions.

The model inorganic foulant (ST-XL) measured 60.7 ± 1.2 nm in hydrodynamic diameter and had a high negative surface zeta potential ($\zeta = -37.9 \pm 0.4$ mV) under experimental conditions. These results agree with the manufacturer's specifications of size (between 40 and 60 nm) and previously published zeta potential measurements [15]. The measured particle sizes of dextran, BSA and sodium alginate were all one order of magnitude smaller than that of ST-XL indicating that they can penetrate the ST-XL colloidal cake layer during filtration. Particle size is not reported for HA because its extremely small size (~1 nm) is beyond the detection range for DLS measurement.

Table 1
Characteristics of model foulants[a].

Model foulant	Zeta potential (mV)	Diameter (nm)
Dextran	−7.2 ± 1.5	4.3 ± 0.2
BSA	−20.7 ± 0.9	6.9 ± 0.2
Humic acid	−37.9 ± 1.2	n/a
Sodium alginate	−45.0 ± 1.2	5.12 ± 2.2
Silica (ST-XL)	−37.9 ± 0.4	60.7 ± 1.2

[a] Reported values are the average of five measurements with standard deviation. The solution condition used was 10 mM NaCl and pH 5.9 ± 0.3.

4.2. Adsorption of organic foulants on silica surface

QCM-D experiments were performed using silica-coated crystal sensors to investigate adsorption of the model organic foulants on the silica surface. Adsorption is indicated by changes in the vibration frequency of the piezoelectric quart-crystal sensor, and the amount of organic molecules adsorbed can be calculated from the frequency change using the Sauerbrey equation [39] (Eq. (6)) provided that the adsorbed layer is rigid, indicated by low energy dissipation:

$$\Delta f = -\frac{2f_0^2}{A\sqrt{\rho_q \mu_q}} \Delta m \tag{6}$$

where Δf is change in frequency (Hz), f_0 is the resonant frequency (Hz) of the crystal sensor, Δm is change in mass adsorbed (kg), A is the piezoelectrically active crystal area (m^2), ρ_q is the density of quartz (kg/m^3), and μ_q is the shear modulus of quartz (Pa).

Experiments using dextran, HA, and sodium alginate showed negligible change in the vibration frequency of the silica-coated crystal sensor, indicating no adsorption of these compounds on the silica surface. This is consistent with the very high negative zeta potentials of humic acid and alginate (Fig. 3) and consequently strong electrostatic repulsion between these molecules and the negatively charged silica surface.

Significant adsorption of BSA on silica surface was observed. Fig. 2 presents the areal mass of BSA adsorbed as well as the thickness of the adsorbed layer, calculated from the Sauerbrey equation. A comparison of the Sauerbrey model fit to that by a visco-elastic model [37] indicates that a rigid layer is adsorbed and that the Sauerbrey equation is valid. The calculated thickness of the adsorbed layer indicates a monolayer of BSA adsorbed on the surface of the silica-coated crystal, suggesting that the presence of BSA may change the surface properties of the silica colloids and hence their interactions with the membrane and other silica colloids.

4.3. Impact of the organic foulants on the physicochemical properties of silica colloids

Adsorption of dissolved organic compounds on the surface of ST-XL may alter its surface properties, e.g., zeta potential and particle size, and consequently impact the interactions among ST-XL colloids. Surface zeta potential and hydrodynamic diameter of ST-XL were measured in the presence and absence of the model organic

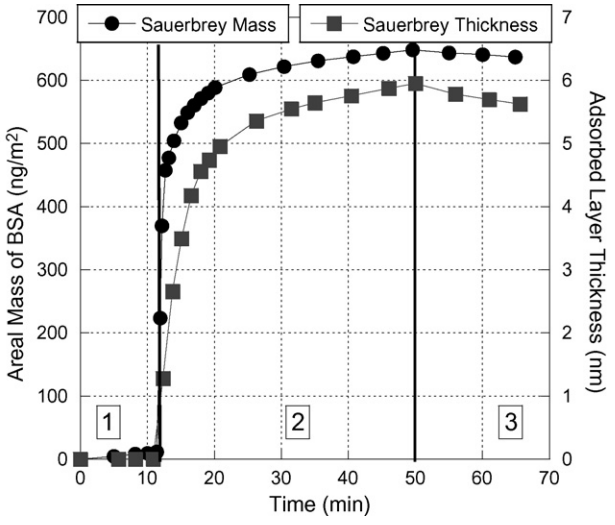

Fig. 2. Areal mass and thickness of the adsorbed BSA layer on the silica surface. Phase 1: 10 mM NaCl; phase 2: 20 mg/L BSA in 10 mM NaCl; phase 3: 10 mM NaCl.

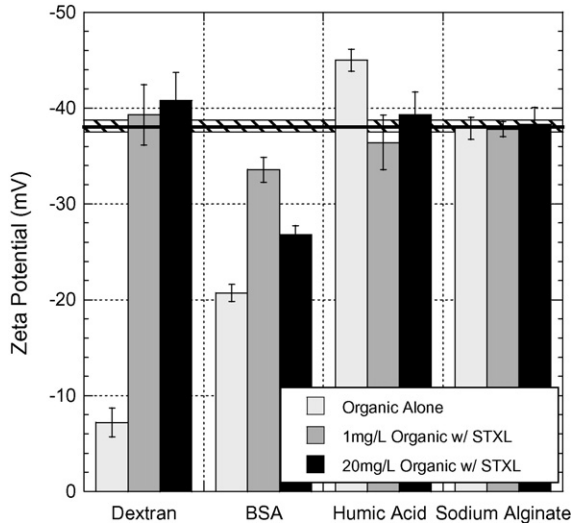

Fig. 3. Surface zeta potential of ST-XL in the presence of varying concentrations of model organic foulants. Horizontal black line with striped halo represents the average and standard deviation of ST-XL surface zeta potential in the absence of model organic foulants. All test solutions contained 10 mM NaCl and the pH was 5.9 ± 0.3.

foulants, and the influence of the model organics under relevant solution conditions is demonstrated in Figs. 3 and 4.

It is worth noting that although electrophoretic mobility measurement using phase analysis light scattering provides an average zeta potential of all particles in a suspension, the size and concentration (1 or 20 mg/L) of dissolved organic compounds in the mixed suspensions were so small that the free organic molecules in the mixture had negligible impact on the zeta potential of the suspension. Zeta potential measurements of the organic foulants alone at these concentrations yielded non-detectable signals. The zeta potential and size of the organic foulants reported in Table 1 were achieved using much higher concentrations: at least 100 mg/L for HA and 1 g/L for dextran, alginate and BSA. Therefore, it is safe to consider that the measured zeta potential or mean particle size of the mixed suspensions represents that of the ST-XL with or without the model organic foulants adsorbed on the surface.

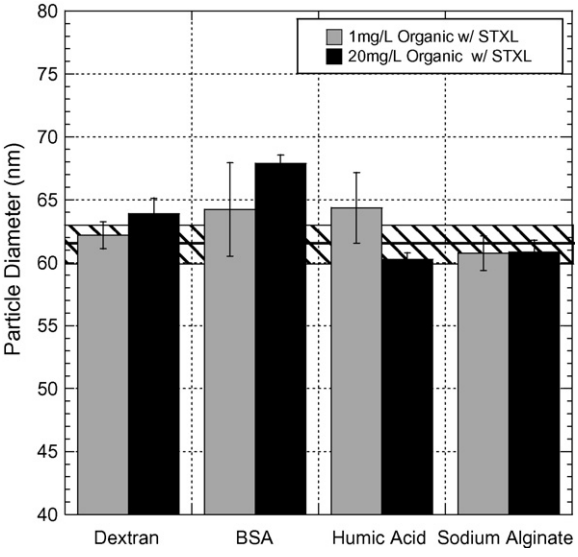

Fig. 4. Particle size of ST-XL in the presence of varying concentrations of model organic foulants. Black line with striped halo represents the average and standard deviation of the measured particle size of ST-XL in the absence of model organic foulants. All test solutions contained 10 mM NaCl, and the pH was 5.9 ± 0.3.

As shown in Fig. 3, the zeta potential of the ST-XL was not affected by dextran or HA despite the zeta potentials of both dextran and HA being very different from that of the silica colloids. Meanwhile, no significant changes in particle size were observed in the presence of these two organic compounds (Fig. 4), indicating no adsorption of HA dextran on the ST-XL colloidal surface. Similarly, no significant change in zeta potential or particle size of the ST-XL colloids is observed in the presence of alginate. This is consistent with the QCM-D measurements that showed no adsorption of these compounds on silica-coated quartz crystal sensors.

In the presence of the model protein BSA, however, the magnitude of the zeta potential of the silica colloids decreased notably and the reduction increased with increasing BSA concentration (Fig. 3). In addition, a careful examination of the particle size of ST-XL suggests the presence of an adsorbed BSA layer (Fig. 4). In the presence of 20 mg/L of BSA, the diameter of ST-XL increased by approximately 7 nm. The reduced zeta potential and increase particle size are consistent with the adsorption of a monolayer BSA on the silica surface observed in the QCM-D experiments. Data in Figs. 3 and 4 also indicate that surface coverage of BSA increases with BSA concentration.

4.4. Impact of the organic foulants on membrane surface zeta potential

The zeta potential of the NF 270 membrane in 10 mM NaCl solution at pH 5.0 is −23.6 ± 1.5 mV. Membrane surface zeta potential measurements in the presence of each model foulant were performed immediately after those without organic foulants using the same membrane coupons. Fig. 5 illustrates the effect of the four model organic foulants on the membrane surface zeta potential. Changes in the membrane surface zeta potential upon exposure to the organic foulants are presented. Negative values indicate reduction in the negative zeta potential, while positive values represent increases.

All model organic foulants except dextran caused notable changes in membrane surface zeta potential, indicating significant adsorption of BSA, alginate and HA on the membrane surface. While adsorption of the highly negatively charged HA and alginate led to an increase in the magnitude of the negative membrane surface zeta potential, BSA significantly reduced its magnitude due to its lower charge density. These changes suggest that HA and alginate

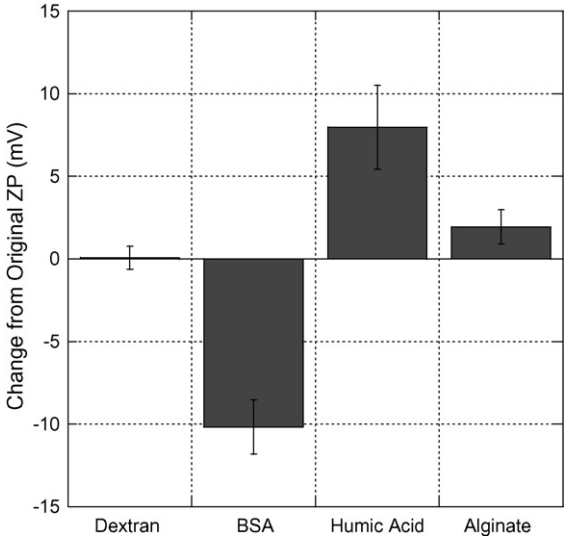

Fig. 5. Effect of organic foulants on membrane surface zeta potential (10 mM NaCl, pH 5.2 ± 5.5). Values represent the change from the original membrane zeta potential of −23.6 ± 1.5 mV.

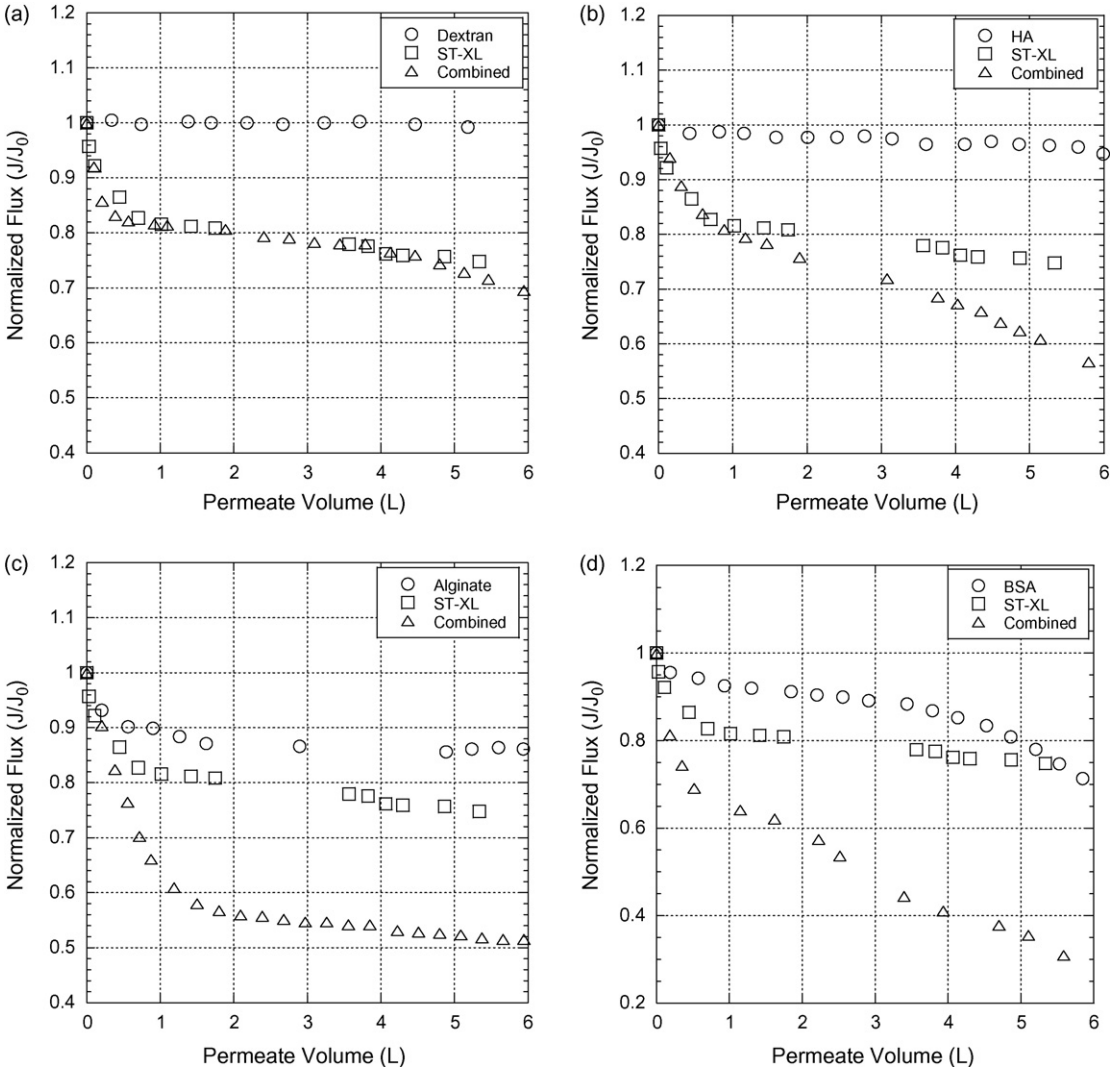

Fig. 6. Normalized flux of the individual organic and colloidal fouling and the combined fouling experiments for, (a) dextran; (b) humic acid; (c) sodium alginate; and (d) BSA.

will increase the electrostatic repulsion between the membrane and the ST-XL colloids, while BSA will have an opposite effect.

4.5. Cross-flow filtration results

Fouling experiments were performed with feed waters containing ST-XL alone, an organic foulant alone and both the ST-XL and an organic foulant. Concentrations of ST-XL and the organic foulants were 100 and 20 mg/L, respectively, in all experiments. Fig. 6 shows the membrane permeate flux measured in all four sets of experiments, each with a different model organic foulant.

In order to examine the three proposed combined fouling mechanisms, the combined fouling layer resistance was compared to that predicted from the individual foulant resistance using a resistance in series model. The predicted value, calculated by summing the resistances of the individual colloidal and organic fouling layers, is referred as "the sum" in the discussion hereafter.

The resistance of the fouling layer was calculated using a rearrangement of Darcy's Law (Eq. (1)), where the trans-membrane osmotic pressure ($\Delta\pi_m$) was calculated following a previously published method [9,18]. Rearranging the film-theory equation produces the following expression [9],

$$\Delta\pi_m = f_{os}(C_m - C_p) = f_{os}C_bR_o \exp\left(\frac{v}{k}\right) \quad (7)$$

which relates the trans-membrane osmotic pressure to the bulk molar salt concentration (C_b), the observed salt rejection ($R_o = 1 - C_p/C_b$), and the mass-transfer coefficient (k) through the osmotic coefficient f_{os} [40]. Since low salt concentrations were used in this study, van't Hoff's equation was used to determine f_{os} [18].

As the experiments were performed under laminar conditions, the initial mass-transfer coefficient, k_0, was calculated during the conditioning phase using Eq. (8),

$$k_0 = 0.808\left(\frac{6QD_\infty^2}{WH^2L}\right)^{1/3} \quad (8)$$

Here D_∞ is the bulk diffusion coefficient of the solute, Q is the volumetric feed flow rate, W is the channel width, H is the channel height, and L is the channel length. Plugging values of the initial permeate flux v_o, k_o and the observed salt rejection R_o during the conditioning stage into the second half of Eq. (7) allows calculation of the intrinsic salt rejection R_i ($R_i = 1 - C_p/C_m$). $\Delta\pi_m$ during the fouling experiment was then calculated using the first half of Eq. (7) from the measured C_p assuming a constant R_i.

Observed salt rejection during colloidal fouling alone decreased slightly from 55.0 to 52.1% (Fig. 8), which agrees well with the modeling results of calculated CECP for the NF270 membrane [9,18]. These results show that silica colloid cake-enhanced concentration

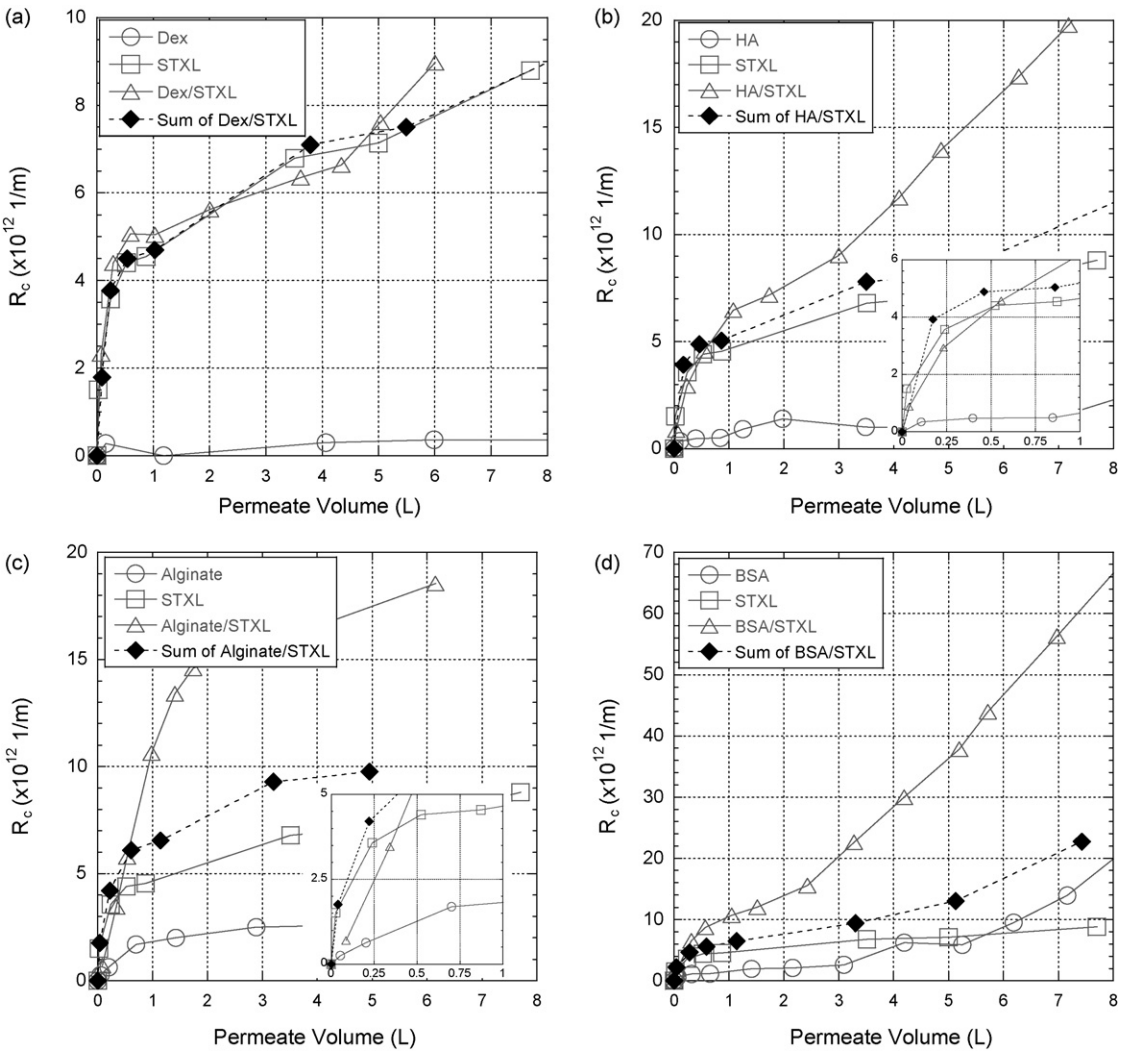

Fig. 7. Calculated cake/gel layer resistances (R_c) of each fouling experiment compared to the sum of individual foulant contribution for (a) dextran; (b) humic acid; (c) sodium alginate; and (d) BSA.

polarization has negligible contribution to the flux decline of the NF270 membrane due to its low salt rejection. Therefore, contrary to other studies [15], CECP as a combined fouling mechanism will not be discussed here.

Fig. 7 compares the calculated cake/gel layer resistances for each set of fouling experiments. The resistances are plotted as a function of cumulative permeate volume. This normalizes the plots, as the amount of colloidal or organic foulant transported to the membrane surface at a given permeate volume during the combined fouling experiment should be the same as that during colloidal fouling or organic fouling experiment if there are no organic-silica interactions.

The flux decline rates during the initial stage of fouling for all experiments are summarized in Table 2. Salt rejections during selected experiments are presented in Fig. 8. The effect of each organic foulant is discussed below.

4.5.1. Combined fouling with dextran

Fig. 6a compares the membrane flux during filtration of the dextran solution, the ST-XL suspension and the mixture of dextran and ST-XL. The corresponding fouling layer resistances for these experiments are plotted in Fig. 7a.

Dextran alone did not foul the membrane, as evidenced by the stable membrane flux throughout the organic fouling experiment. The ST-XL colloids caused significant decline of the membrane flux. Up until the latter stages of fouling, combined fouling with dextran creates a similar fouling layer resistance as that with silica alone. Towards the end of the experiment, however, the combined cake layer resistance begins to rapidly increase compared to the sum term, indicating a synergistic effect. Since dextran does not adsorb on ST-XL, the observed synergy indicates that both hindered back diffusion and a change in cake layer structure are present. Because this change in resistance is seen in the latter stages of fouling after significant accumulation of foulants has occurred, it is likely that the increase in resistance is caused by a change in cake layer structure as dextran fills in the interstitial pore space of the cake layer and

Table 2
Initial flux decline rates of all fouling experiments.

Foulant(s)	Initial flux decline rate[a] (L^{-1})
ST-XL	0.77
Dextran	0.02
Dextran + ST-XL	0.81
Humic acid	0.04
Humic acid + ST-XL	0.39
Sodium alginate	0.25
Alginate + ST-XL	0.44
BSA	0.16
BSA + ST-XL	1.07

[a] The initial flux decline rate is calculated by fitting data collected during the first 100 min by a linear function assuming $J/J_o = 1$.

that hindered back diffusion remains a small but contributive effect during combined fouling with dextran.

4.5.2. Combined fouling with HA

As shown in Fig. 6b, fouling by HA alone caused only slight flux decline. The combined fouling experiment with HA and ST-XL showed no synergistic effect in the beginning stage. In fact, a closer look at the initial flux decline rates (Table 2) during filtration of the ST-XL suspension and the mixture of HA and ST-XL (0.77 and 0.39 L^{-1}, respectively) shows that the presence of HA reduced the initial flux decline rate. This is attributed to HA adsorption onto the membrane surface, which increases the electrostatic repulsion between the foulants and the membrane. In the latter fouling stages, however, the membrane flux during combined fouling deviated from the calculated sum and showed a synergistic effect that continued to increase with filtration time. As HA does not adsorb to ST-XL, this increase is either due to the hindered back diffusion effect or to the increased resistance caused by a mixed fouling layer with HA interspersed in the ST-XL cake layer.

4.5.3. Combined fouling with sodium alginate

Initial flux decline in the presence of sodium alginate alone was the most substantial of all the organic foulants (Fig. 6c). The alginate fouling layer also displayed active salt rejecting characteristics, as evidenced by the steady increase in observed salt rejection over the length of the experiment (Fig. 8). Strong synergism was observed during the filtration of the ST-XL-alginate mixture (Fig. 7c). The fouling layer resistance calculated during combined fouling is significantly higher than the calculated sum of individual fouling layers in spite of the slightly reduced initial fouling rate (Table 2, 0.77 L^{-1} vs. 0.44 L^{-1}) caused by the increased repulsion between ST-XL and the membrane. Salt rejection during the combined fouling experiment remained stable over time, indicating either the impact of CECP and salt rejection by the fouling layer were negligible, or the two effects cancelled each other out. The same combined fouling mechanisms for HA (hindered back diffusion and cake layer structure) are expected to apply to alginate. However, the synergistic effect caused by sodium alginate is greater in the initial stages of filtration compared to that by HA. It is postulated that this is due to a more significant effect of the hindered back diffusion mechanism. Since sodium alginate solution is much more viscous than the other model foulants, the back diffusion of the ST-XL colloids in the CP layer may be more severely hindered, causing faster accumulation of ST-XL and therefore a greater flux decline rate.

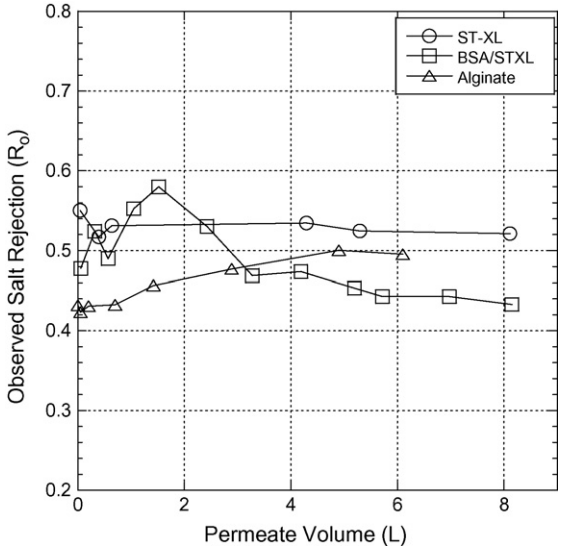

Fig. 8. Salt rejections observed during selected filtration experiments.

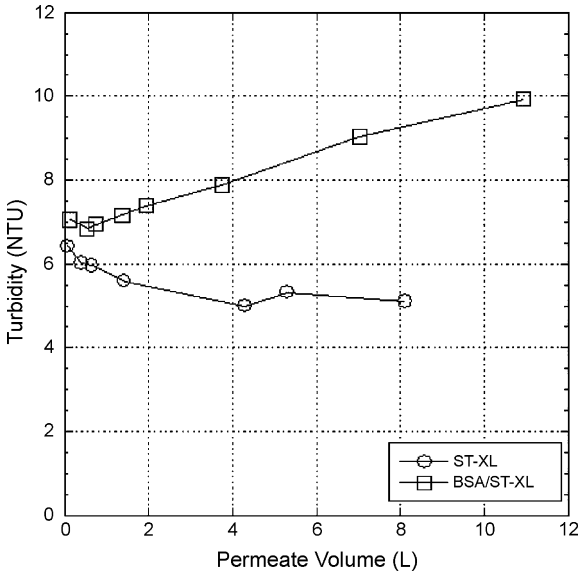

Fig. 9. Feed solution turbidity measurements of selected filtration experiments.

4.5.4. Combined fouling with BSA

Flux decline in the presence of BSA alone appears to be caused by a compressible fouling layer that increases in resistance over time (Fig. 6d). The mixture of BSA and ST-XL caused much greater flux decline than the sum of the contribution from each foulant (Fig. 7d). The greater initial flux decline rate can be explained by the faster deposition of ST-XL due to the reduced electrostatic repulsion between ST-XL and the membrane as well as that between ST-XL colloids, a result of the lower negative surface zeta potential upon adsorption of BSA (Figs. 3 and 5). Analysis of the feed water showed an increase, instead of the expected decrease, in turbidity with filtration time, resulting from the formation of ST-XL aggregates (Fig. 9). Storage of the same feed solution over time did not show similar increase in particle size, indicating that these aggregates likely formed in the CP or fouling layer. This observation suggests that the cake layer formed was dynamic and some ST-XL aggregates were washed off from the membrane surface during cross-flow filtration. This is consistent with the large fluctuation of salt rejection observed during the combined fouling experiment (Fig. 8). While it is unclear if the decrease in salt rejection is due to CECP or a disturbance in the fouling layer, calculations show that the increase in trans-membrane osmotic pressure over the course of the experiment has a negligible contribution to flux decline.

The synergism during the combined fouling experiment continued throughout the experiment. Because BSA adsorbs on silica surfaces, the observed synergism results from the interplay of all the three combined fouling mechanisms discussed in the Theory. In addition, the observed aggregation of foulants in the cake layer as well as the change in the growth rate of the combined fouling layer resistance at permeate volume of about 2.5 L (Fig. 7d) suggests a shift in the combined fouling layer structure towards the latter stages of filtration. These results with BSA show that the effects of organic foulant adsorption on silica surface are complex and can have important implications on membrane flux decline.

5. Conclusions

The flux decline behavior of a nanofiltration membrane in the presence of four model organic macromolecules and one model

silica colloidal foulant was investigated to examine mechanisms responsible for the synergism observed in combined fouling. All model organic foulants tested exhibited a synergistic effect when in combination with the model silica colloids. The extent of the synergy, however, strongly depends on the molecular characteristics of the organic foulant. The three hypothesized mechanisms: increased resistance of the mixed fouling layer, hindered back diffusion, and organic foulant adsorption were shown to have varying effects on combined fouling, depending on the specific organic foulant. The greatest synergism was observed in the presence of an interacting organic foulant, BSA, which can adsorb on silica colloids as well as the membrane surface to reduce repulsive interaction between foulants and the membrane as well as that among foulants. Adsorption of the organic foulant to the clean membrane surface only impacts the very beginning fouling stage and does not have a lasting effect on the overall flux decline behavior. The study also showed that the interplay of the various mechanisms in combined fouling can be very complex, calling for further investigation of the combined fouling process. More comprehensive models that incorporate the combined fouling mechanisms suggested here are needed to properly predict the fouling of complex solutions.

Acknowledgements

We thank the National Science Foundation (Awards CBET-0552413 and CBET-0449431) for funding this study. We also thank Candace Marbury and Andrew Kuehler for their assistance in collecting some of the experimental data.

References

[1] T.-H. Bae, I.-C. Kim, T.-M. Tak, Preparation and characterization of fouling-resistant TiO_2 self-assembled nanocomposite membranes, Journal of Membrane Science 275 (1–2) (2006) 1–5.
[2] M. Elimelech, et al., Role of membrane surface morphology in colloidal fouling of cellulose acetate and composite aromatic polyamide reverse osmosis membranes, Journal of Membrane Science 127 (1) (1997) 101–109.
[3] J.E. Kilduff, et al., Photochemical modification of poly(ether sulfone) and sulfonated poly(sulfone) nanofiltration membranes for control of fouling by natural organic matter, Desalination 132 (1–3) (2000) 133–142.
[4] I.C. Kim, Y.H. Ka, J.Y. Park, K.H. Lee, Preparation of fouling resistant nanofiltration and reverse osmosis membranes and their use for dyeing wastewater effluent, Journal of Industrial & Engineering Chemistry 10 (1) (2004) 115–121.
[5] S.R. Baggott, A. Jaffer, The application of a novel chemical treatment program to mitigate scaling and fouling in reverse osmosis units, Desalination 83 (1–3) (1991) 119.
[6] T. Leiknes, H. Ødegaard, H. Myklebust, Removal of natural organic matter (NOM) in drinking water treatment by coagulation-microfiltration using metal membranes, Journal of Membrane Science 242 (1–2) (2004) 47–55.
[7] R.Y. Ning, T.L. Troyer, R.S. Tominello, Chemical control of colloidal fouling of reverse osmosis systems, Desalination 172 (1) (2005) 1–6.
[8] W. Song, et al., Nanofiltration of natural organic matter with H_2O_2/UV pretreatment: fouling mitigation and membrane surface characterization, Journal of Membrane Science 241 (1) (2004) 143–160.
[9] E.M.V. Hoek, A.S. Kim, M. Elimelech, Influence of crossflow membrane filter geometry and shear rate on colloidal fouling in reverse osmosis and nanofiltration separations, Environmental Engineering Science 19 (6) (2002) 357–372.
[10] C.Y. Tang, Y.-N. Kwon, J.O. Leckie, Fouling of reverse osmosis and nanofiltration membranes by humic acid—effects of solution composition and hydrodynamic conditions, Journal of Membrane Science 290 (1–2) (2007) 86–94.
[11] G. Foley, D.M. Malone, F. MacLoughlin, Modelling the effects of particle polydispersity in crossflow filtration, Journal of Membrane Science 99 (1) (1995) 77–88.
[12] D.E. Potts, R.C. Ahlert, S.S. Wang, A critical review of fouling of reverse osmosis membranes, Desalination 36 (3) (1981) 235–264.
[13] H.B. Dharmappa, et al., A comprehensive model for cross-flow filtration incorporating polydispersity of the influent, Journal of Membrane Science 65 (1–2) (1992) 173–185.
[14] S. Lee, M. Elimelech, Relating organic fouling of reverse osmosis membranes to intermolecular adhesion forces, Environmental Science & Technology 40 (3) (2006) 980–987.
[15] S. Lee, J.W. Cho, M. Elimelech, Combined influence of natural organic matter (NOM) and colloidal particles on nanofiltration membrane fouling, Journal of Membrane Science 262 (1–2) (2005) 27–41.
[16] Q. Li, M. Elimelech, Synergistic effects in combined fouling of a loose nanofiltration membrane by colloidal materials and natural organic matter, Journal of Membrane Science 278 (1–2) (2006) 72–82.
[17] A.I. Schäfer, et al., Microfiltration of colloids and natural organic matter, Journal of Membrane Science 171 (2) (2000) 151–172.
[18] E.M.V. Hoek, M. Elimelech, Cake-enhanced concentration polarization: a new fouling mechanism for salt-rejecting membranes, Environmental Science & Technology 37 (24) (2003) 5581–5588.
[19] A.S. Kim, A.N.L. Ng, Hydraulic permeability of polydispersed cake layers: an analytic approach, Desalination 207 (1–3) (2007) 144–152.
[20] V.V. Tarabara, et al., Morphology of deposits formed from chemically heterogeneous suspensions: application to membrane filtration, Journal of Colloid and Interface Science 256 (2) (2002) 367–377.
[21] A.S.L. Kim, Y. Liu, Irreversible chemical potential and shear-induced diffusion in crossflow filtration, Industrial Engineering and Chemistry Research 47 (15) (2008) 5611–5614.
[22] G. Belfort, R.H. Davis, A.L. Zydney, The behavior of suspensions and macromolecular solutions in crossflow microfiltration, Journal of Membrane Science 96 (1–2) (1994) 1–58.
[23] A. Amirbahman, T.M. Olson, Transport of humic matter-coated hematite in packed beds, Environmental Science & Technology 27 (13) (1993) 2807–2813.
[24] R. Kretzschmar, H. Sticher, Transport of humic-coated iron oxide colloids in a sandy soil: influence of Ca^{2+} and trace metals, Environmental Science & Technology 31 (12) (1997) 3497–3504.
[25] R.A.D.J. Akbour, M. Hamdani, P. Schmitz, Transport of kaolinite colloids through quartz sand: influence of humic acid, Ca^{2+}, and trace metals, Journal of Colloid and Interface Science 253 (1) (2002) 1–8.
[26] K.L. Chen, M. Elimelech, Influence of humic acid on the aggregation kinetics of fullerene (C60) nanoparticles in monovalent and divalent electrolyte solutions, Journal of Colloid and Interface Science 309 (1) (2007) 126–134.
[27] E.M. Vrijenhoek, S. Hong, M. Elimelech, Influence of membrane surface properties on initial rate of colloidal fouling of reverse osmosis and nanofiltration membranes, Journal of Membrane Science 188 (1) (2001) 115–128.
[28] C. Bellona, J.E. Drewes, The role of membrane surface charge and solute physicochemical properties in the rejection of organic acids by NF membranes, Journal of Membrane Science 249 (1–2) (2005) 227–234.
[29] A.E. Childress, M. Elimelech, Effect of solution chemistry on the surface charge of polymeric reverse osmosis and nanofiltration membranes, Journal of Membrane Science 119 (2) (1996) 253–268.
[30] H. Mo, K.G. Tay, H.Y. Ng, Fouling of reverse osmosis membrane by protein (BSA): effects of pH, calcium, magnesium, ionic strength and temperature, Journal of Membrane Science 315 (1–2) (2008) 28–35.
[31] D.J. Barker, D.C. Stuckey, A review of soluble microbial products (SMP) in wastewater treatment systems, Water Research 33 (14) (1999) 3063–3082.
[32] C. Jarusutthirak, G. Amy, J.-P. Croué, Fouling characteristics of wastewater effluent organic matter (EfOM) isolates on NF and UF membranes, Desalination 145 (1–3) (2002) 247–255.
[33] C. Jarusutthirak, G. Amy, Understanding soluble microbial products (SMP) as a component of effluent organic matter (EfOM), Water Research 41 (12) (2007) 2787–2793.
[34] K.J. Howe, M.M. Clark, Fouling of microfiltration and ultrafiltration membranes by natural waters, Environmental Science & Technology 36 (16) (2002) 3571–3576.
[35] A.D. Levine, G. Tchobanoglous, T. Asano, Characterization of the size distribution of contaminants in waste-water-treatment and reuse implications, Journal of Water Pollution Control Federation 57 (1985) 805.
[36] G.G. Leppard, D. Mavrocaordatos, D. Perret, Electron-optical characterization of nano- and micro-particles in raw and treated waters: an overview, Water Science Technology 50 (2004) 1.
[37] F. Höök, Development of a Noval QCM Technique for Protein Adsorption Studies, in Department of Biochemistry and Biophysics and Department of Applied Physics, Chalmers University of Technology, Götebory University, Göteborg, Sweden, 1997, p. 60.
[38] Q. Li, Z. Xu, I. Pinnau, Fouling of reverse osmosis membranes by biopolymers in wastewater secondary effluent: role of membrane surface properties and initial permeate flux, Journal of Membrane Science 290 (1–2) (2007) 173–181.
[39] G. Sauerbrey, Verwendung von Schwingquarzen zur Wagung diinner Schicten und zur Mikrowagung, Zeitschrift Fur Physik 155 (1959) 206–222.
[40] L. Song, et al., Performance limitation of the full-scale reverse osmosis process, Journal of Membrane Science 214 (2) (2003) 239–244.